Title

The Chiral Potential of Phenanthriplatin and Its Influence on Guanine Binding

Journal

Journal of the American Chemical Society, 136(5)

ISSN

0002-7863

Authors

Johnstone, Timothy C

Lippard, Stephen J

Publication Date

2014-02-05

DOI

10.1021/ja4125115

Peer reviewed

JACS
JOURNAL OF THE AMERICAN CHEMICAL SOCIETY
Article
pubs.acs.org/JACS

The Chiral Potential of Phenanthriplatin and Its Influence on Guanine Binding

Timothy C. Johnstone and Stephen J. Lippard*

Department of Chemistry, Massachusetts Institute of Technology, Cambridge, Massachusetts 02139, United States

Supporting Information

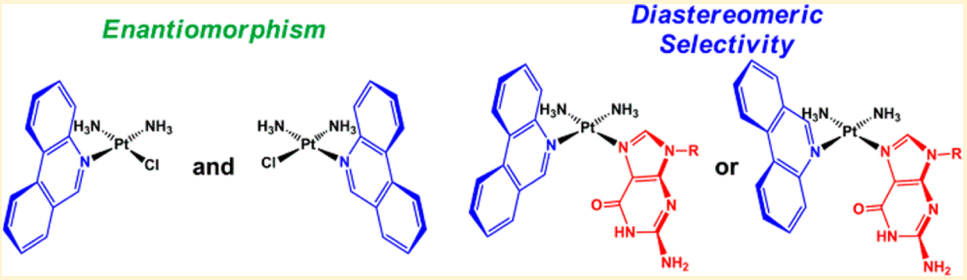

ABSTRACT: The monofunctional platinum complex *cis*-$[Pt(NH_3)_2Cl(Am)]^+$, also known as phenanthriplatin, where Am is the *N*-heterocyclic base phenanthridine, has promising anticancer activity. Unlike bifunctional compounds such as cisplatin, phenanthriplatin can form only one covalent bond to DNA. Another distinguishing feature is that phenanthriplatin is chiral. Rotation about the Pt−N bond of the phenanthridine ligand racemizes the complex, and the question arises as to whether this process is sufficiently slow under physiological conditions to impact its DNA-binding properties. Here we present the results of NMR spectroscopic, X-ray crystallographic, molecular dynamics, and density functional theoretical investigations of diastereomeric phenanthriplatin analogs in order to probe the internal dynamics of phenanthriplatin. These results reveal that phenanthriplatin rapidly racemizes under physiological conditions. The information also facilitated the interpretation of the NMR spectra of small molecule models of phenanthriplatin-platinated DNA. These studies indicate, inter alia, that one diastereomeric form of the complexes *cis*-$[Pt(NH_3)_2(Am)(R\text{-}Gua)]^{2+}$, where R-Gua is 9-methyl- or 9-ethylguanine, is preferred over the other, the origin of which stems from an intramolecular interaction between the carbonyl oxygen of the platinated guanine base and a *cis*-coordinated ammine. The relevance of this finding to the DNA-damaging properties of phenanthriplatin and its biological activity is discussed.

INTRODUCTION

Platinum drugs are a mainstay of cancer therapy. Approximately half of all cancer patients receiving chemotherapy are given a platinum-containing drug.[1] Cisplatin, carboplatin, and oxaliplatin (Chart 1) − three platinum complexes approved by the US FDA for the treatment of human cancer − are commonly applied to treat bladder, testicular, head and neck, ovarian, colon, and small cell and nonsmall cell lung cancers.[2] Despite such widespread use, these treatments are accompanied by a number of shortcomings.[3] The cytotoxicity of these drugs is not limited to cancer cells, and off-target activity results in emesis, alopecia, nausea, kidney damage, myelosuppression, and peripheral neuropathy. Moreover, many tumors are either inherently resistant to the currently employed platinum-based therapies or acquire resistance during treatment. In an attempt to find molecules with improved potency, fewer side effects, and a novel spectrum of activity, researchers have prepared thousands of platinum complexes and tested them for anticancer activity. One strategy used to address the foregoing issues is to devise complexes that depart from the neutral, square-planar, DNA-cross-linking *cis*-dia(m)mine−platinum(II) paradigm that has long dominated the field.[4] A current manifestation explores cationic monofunctional platinum(II) complexes,[5] which bear only one labile ligand and form one bond to the DNA nucleobases. The significant difference in the interaction of monofunctional complexes with DNA compared to classical bifunctional cross-linking compounds very likely contributes to the unique response that phenanthriplatin, or *cis*-$[Pt(NH_3)_2(phenanthridine)Cl]^+$ (Chart 1), elicits when used to treat cancer cells.[6] Studies with the monofunctional compound pyriplatin (Chart 1), *cis*-$[Pt(NH_3)_2(pyridine)Cl]^+$, reveal that little distortion of the DNA double helix is induced upon platination,[7] and a similar situation is likely to be obtained with phenanthriplatin. This result is very different from the significant DNA bending at 1,2-intrastrand cross-links that occurs following treatment with bifunctional platinum agents such as cisplatin.[8]

Crystallographic and biochemical studies have revealed the mechanism by which pyriplatin exerts its anticancer activity, most likely transcription inhibition followed by consequent apoptosis.[7,9,10] Structural studies suggest that the steric bulk of

Received: December 9, 2013
Published: January 13, 2014

   dx.doi.org/10.1021/ja4125115 | J. Am. Chem. Soc. 2014, 136, 2126−2134

Chart 1. Bifunctional and Monofunctional Platinum Anticancer Agents[a]

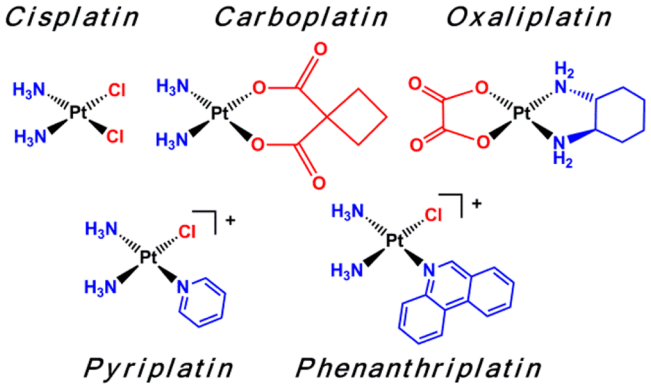

[a]Nonleaving group ligands are colored blue, and leaving group ligands are red.

the pyridine ring is crucial for activity.[9] This hypothesis provides an explanation for the contrast between the activity of pyriplatin and the inactivity previously observed for monofunctional compounds such as $[Pt(NH_3)_3Cl]^+$ and $[Pt(dien)Cl]^+$.[11] A systematic variation of the *N*-heterocyclic ring Am in compounds of the form *cis*-$[Pt(NH_3)_2(Am)Cl]^+$ resulted in the discovery of the far more potent analog phenanthriplatin.[6,12] In a preliminary screen of cultured human cancer cells, phenanthriplatin displayed significantly greater cytotoxicity than cisplatin and showed a pattern of activity distinct from that of either cisplatin/carboplatin or oxaliplatin. A more detailed understanding of the spectrum of activity was gained by analyzing the cytotoxicity of phenanthriplatin in the NCI60 panel of cancer cells. The pattern of cell killing was uncorrelated with that of any other platinum agent in the NCI database. Unlike pyriplatin, the asymmetry of the phenanthridine ring renders phenanthriplatin chiral. That phenanthriplatin can exist as two distinct enantiomers is of potential importance because the two enantiomers may display different pharmaceutical activity.

Nuclear DNA is the presumed target of most platinum anticancer agents.[13] Initial experiments revealed that phenanthriplatin binds DNA and that it does so in a covalent, rather than intercalative, manner.[6] Moreover, studies with *E. coli*, analogous to those initially performed to investigate the mechanism of action of cisplatin, corroborate the hypothesis that the interaction of phenanthriplatin with DNA is responsible for its anticancer effects.[14]

To gain more insight into the nature of the interaction of phenanthriplatin with DNA, we prepared small molecule complexes that model its reactions with guanosine residues (Chart 2).

The N7 position of guanine is the most nucleophilic among DNA bases and, as a result, it is the primary binding site for platinum agents.[15] The model complexes *cis*-$[Pt(NH_3)_2(R\text{-}Gua)(Am)](OTf)_2$, where R-Gua is a 9-alkylguanine, Am is phenanthridine, and OTf is trifluoromethanesulfonate or triflate, were therefore prepared using the triflate salt of phenanthriplatin as a synthetic precursor. The chirality of phenanthriplatin combined with coordination to R-Gua creates diastereomers, the nature of which was investigated by X-ray crystallography and NMR spectroscopy.

Here we report the results of an investigation of these diastereomeric analogs of phenanthriplatin (Chart 2), which were prepared to investigate whether the two phenanthriplatin enantiomers can be resolved on the physiological time scale. These studies reveal that phenanthriplatin rapidly racemizes in solution. Consideration of its dynamics is crucial for interpreting the conformational isomerism observed with the 9-alkylguanine model complexes. Evidence in both the solid state and solution phase indicates that, when phenanthriplatin

Chart 2. Platinum Complexes Investigated in This Article

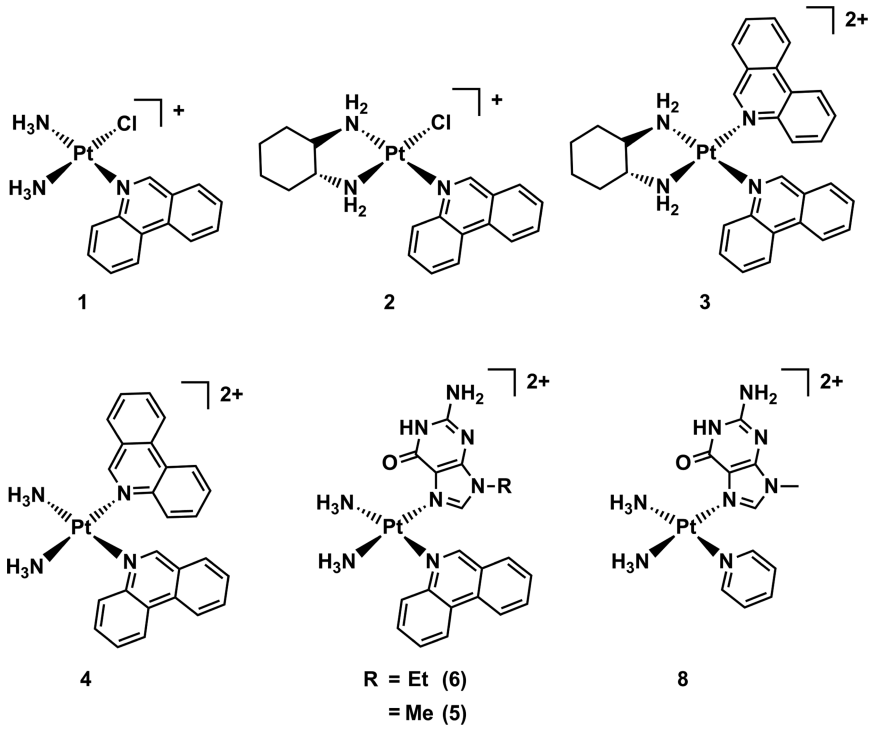

dx.doi.org/10.1021/ja4125115 | J. Am. Chem. Soc. 2014, 136, 2126−2134

reacts with guanine, diastereomeric selection occurs among the possible conformational isomers that can form. The origin of this selection has been identified, as described in this article.

EXPERIMENTAL SECTION

The synthesis and characterization of the compounds under discussion are presented in the Supporting Information along with crystallographic details and specifications of the instruments used for physical measurements.

Line Shape Analysis of Variable Temperature NMR Data. ^{1}H NMR spectra were acquired over a temperature range for **2**−**4** to investigate potential fluxional behavior exhibited by these compounds. The rate of exchange at the temperature at which two peaks coalesce was estimated using eq 1, in which k is the rate of exchange at the coalescence temperature and $\Delta\nu$ is the difference in Hz between the two signals in the low temperature (slow exchange) limit.[16−18] This estimate was used to inform the initial guess in a full line shape analysis. This more detailed analysis was conducted using the *MEXICO* series of computer programs.[19,20] Simulated spectra were fit to experimental spectra at the different temperatures, and the corresponding rate constants were extracted. These rate constants were used to construct Eyring plots and determine activation parameters.

$$k = \frac{\pi\Delta\upsilon}{\sqrt{2}} \tag{1}$$

Nuclear Overhauser Effect NMR Experiments. Deuterated DMSO solutions of **6** and **8**, both of which are 9-methylguanine complexes, were sparged with N_2 for 2 min and then sealed in an NMR tube under a blanket of nitrogen. Saturation transfer experiments were conducted on the deoxygenated samples. Briefly, for each sample, a ^{1}H NMR spectrum was acquired following preirradiation at the frequency of the methylguanine H8 ($H8_G$) resonance. The preirradiation power was chosen so as to just saturate the $H8_G$ signal and eliminate it from the spectrum. A second spectrum was then acquired with identical parameters, but with the saturation frequency set to a region downfield and devoid of signals. The second spectrum was subtracted from the first.

No cross peaks between $H8_G$ and any of the phenanthridine protons were observed in a NOESY experiment. Rotating-Frame Overhauser effect (ROESY) spectra were collected on samples prepared in deoxygenated acetone-d_6. A mixing time of 200 ms was employed with a 90° pulse of 11 μs.

Computational Details. *Molecular Mechanics (MM).* The complex cation of **6** was constructed in *GaussView*, and the planes of the phenanthridine and 9-ethylguanine ligands were set perpendicular to the coordination plane. Two conformers were investigated, one in which the H6 proton of the phenanthridine ligand ($H6_P$) and $H8_G$ were on the same side of the platinum coordination plane and the other in which they were on opposite sides. An MM geometry optimization was carried out for each conformer using *Gaussian03*.[21] The universal force field[22] was employed using technical details described previously.[23]

Density Functional Theory. Geometry optimizations were carried out using *ORCA*.[24] Calculations were carried out using the pure GGA functional, BP86.[25,26] The zero order relativistic approximation (ZORA), along with the attendant TZV-ZORA basis set, was applied to treat relativistic effects.[27] The resolution of the identity approximation and the appropriate auxiliary basis set were used to accelerate computations. The stationary nature of the structures obtained from geometry optimizations was confirmed using numerical frequency calculations. Optimizations were conducted in either the gas phase or in solution by using an implicit conductor-like screening model (COSMO). To model aqueous solvation, the dielectric constant of the polarizable continuum was set to 80.400 and the refractive index to 1.3300. *PyMol* and *Mercury* were used for molecular visualization.

RESULTS

Synthesis and Characterization. Monofunctional complexes having the formula *cis*-$[Pt(NH_3)_2(Am)Cl]^+$, where Am is an *N*-heterocyclic ligand, have previously been obtained as nitrate salts by treating cisplatin, *cis*-$[Pt(NH_3)_2Cl_2]$, with 1 equiv of silver nitrate followed by an equivalent of Am.[6,7,28] Alternatively, *cis*-$[Pt(NH_3)_2(Am)Cl]Cl$ can be obtained by heating cisplatin with Am to displace one of the chloride ligands.[28] A major problem with these methods, however, is that neither silver-mediated halide abstraction nor direct ligand substitution proceeds selectively at just one coordination site. As a result, in addition to the desired *cis*-$[Pt(NH_3)_2(Am)Cl]^+$ complex, appreciable amounts of *cis*-$[Pt(NH_3)_2(Am)_2]^{2+}$ form together with unreacted cisplatin.

Here we use silver triflate to prepare **7** and **1**, triflate salts of pyriplatin and phenanthriplatin, respectively, to provide a much wider range and degree of solubility in organic solvents. As a result, addition of acetone to the residue that remains following removal of DMF from the synthesis mixtures of **1** and **7** dissolves the triflate salts of *cis*-$[Pt(NH_3)_2(Am)Cl]^+$ and *cis*-$[Pt(NH_3)_2(Am)_2]^{2+}$. Unreacted cisplatin, on the other hand, does not dissolve in acetone and can be removed by filtration. When ether is layered onto the acetone filtrate, crystals of *cis*-$[Pt(NH_3)_2(Am)Cl]OTf$ deposit over the course of a few days. These crystals can be harvested before the more soluble *cis*-$[Pt(NH_3)_2(Am)_2]OTf_2$ precipitates, providing access to analytically pure material.

Spectroscopic characterization of these complexes was consistent with that which had been previously reported for the nitrate salts of these cations. The assignment of the peaks in the ^{1}H NMR spectrum of **1** was carried out using a combination of COSY and NOESY spectra (Figure S4). This peak assignment was used to interpret saturation transfer NMR experiments.

The syntheses of **2**−**4** proceeded in an analogous manner. The NMR spectra for these compounds (Figure S19−S22) show a multitude of peaks arising from different rotamers that interconvert slowly on the NMR time scale at room temperature. The syntheses of **5**, **6**, and **8** were achieved by treating either **1** or **7** with an additional equivalent of silver triflate and adding the appropriate 9-alkylguanine.

Line Shape Analysis. As described above, the ^{1}H NMR spectra of **2**−**4** exhibit peak multiplicity as a result of slow to intermediate exchange between conformational isomers. Upon heating, these signals broaden, coalesce, and finally sharpen as the rate of exchange increases. These processes are reversible for all three compounds. Although some regions of the spectra have complex overlapping features, other regions show well-resolved peaks and coalescence events. The line shapes of portions of the ^{1}H NMR spectra of **2**−**4** that showed well-defined, baseline-resolved coalescing signals were simulated. The simulated spectra were fit to the experimental data by varying the rate constant. A two-site model was used for **2** and **4**, and a four-site model was used for **3**. An example of the simulated and experimental data for **4** is shown in Figure 1. Data for all compounds can be found in the Supporting Information (Figures S23−S25).

The variation in rate constant with temperature can be used to determine the activation parameters for the interconversion. The enthalpy and entropy of activation, $\Delta H^{\ddagger}$ and $\Delta S^{\ddagger}$ respectively, are obtained from the first order rate constants using an Eyring analysis (Figure 2). Eyring plots for all the

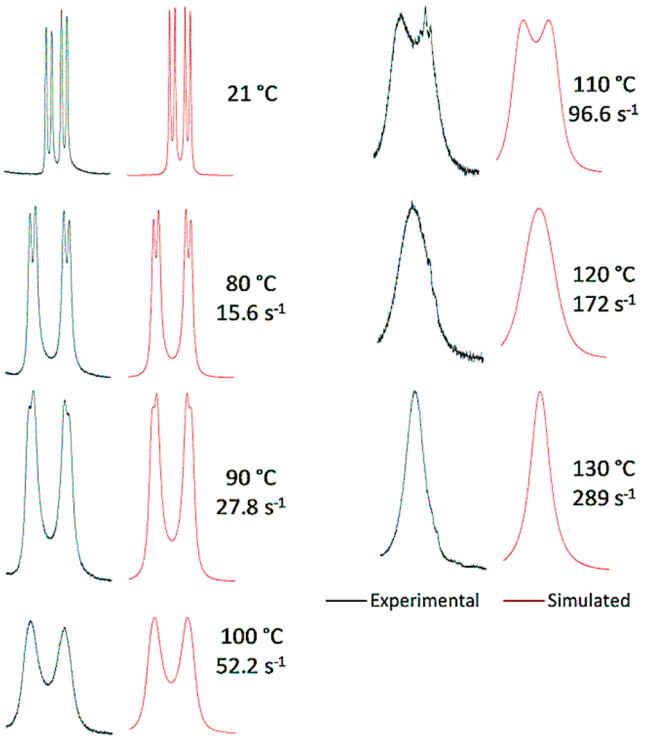

Figure 1. Experimental and simulated line shapes of portions of the ^{1}H NMR spectrum of **4**. The temperature at which the experimental data were collected and the rate constant used to generate the simulation are shown next to each set of data. The signals shown arise from the proton labeled **C** in Figure S7.

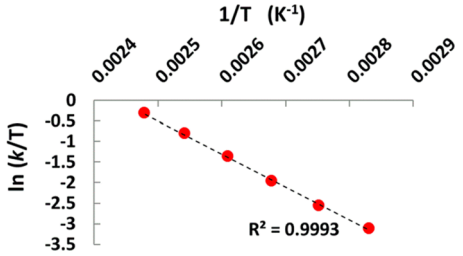

Figure 2. Eyring plot of the conformational isomerism of **4** using the data from Figure 1.

coalescence events simulated are presented in the Supporting Information. The Gibbs free energy of activation at a given temperature T, $\Delta G_T^{\ddagger}$, can be obtained using eq 2.

$$\Delta G_T^{\ddagger} = \Delta H^{\ddagger} - T\Delta S^{\ddagger} \quad (2)$$

$$k_T = \frac{k_b T}{h} e^{-\Delta G_T^{\ddagger}/RT} \quad (3)$$

The values of $\Delta G_{298.15}^{\ddagger}$ for compounds **2**–**4** are collected in Table 1. Using eq 3, where k_b is Boltzmann's constant, h is Planck's constant, and R is the universal gas constant, the rate constant at a given temperature, k_T, can be obtained. The lifetime of the molecule in a given conformational state at temperature T, τ_T, for the process can be obtained by taking the inverse of the rate constant. The values of $\tau_{298.15}$ are also presented in Table 1. The errors for $\Delta G_{298.15}^{\ddagger}$ are obtained by standard propagation of the errors of $\Delta H^{\ddagger}$ and $\Delta S^{\ddagger}$ obtained from the least-squares linear regression Eyring plots. The errors should be taken only as estimates of the true errors and are

Table 1. Free Energies of Activation for Rotation about the Pt–N_P Bond and Lifetimes of Each Conformer[a]

	$\Delta G_{298.15}^{\ddagger}$ (kJ mol^{-1})	$\tau_{298.15}$ (s)
2[b]	70.1(1.7); 70.2(2.2)	0.31; 0.32
3	71.5(1.4)	0.55
4	77.1(1.1)	5.3

[a]See main text for a discussion of the error estimates. [b]Values are presented from determinations using two different coalescence events.

presented to indicate the relative precision with which the different determinations were made. The approximate nature of the error estimate arises from the fact that this analysis treats data across a logarithmic scale on equal footing. Moreover, it equally weights the rate constants from near the coalescence point, which are more accurate, and rate constants obtained far from coalescence, which are less accurate. The error propagation was not carried out for the lifetimes because only modification by physical constants is involved.

X-ray Crystallography. Pertinent crystallographic data for **1**, **5**, **7**, and **8** are summarized in Table S1. Crystallographic data for *trans*-[Pt(pyridine)$_2$Cl$_2$] are presented in the Supporting Information. The crystal structure of **1** (Figure 3) shows the *cis*-[Pt(NH$_3$)$_2$(phenanthridine)Cl]$^+$ cation to be similar in structure to that present in the structure of the nitrate salt,[6] with bond lengths and angles falling within expected ranges. The geometry of the primary coordination sphere in both structures is essentially identical with an RMSD of 0.023 Å. The most significant differences are found in the orientation of the phenanthridine rings as shown in Figure S30. In the nitrate salt, the phenanthridine plane does not contain the line connecting the platinum atom and the nitrogen atoms of the phenanthridine and the *trans* ammine. This line instead forms an angle of 18° with the phenanthridine plane. In the triflate salt, this angle is only 10°. An important aspect of the structure of the complex is that the asymmetry of the phenanthridine ligand about the platinum coordination plane produces a chiral molecule. The space group *Pbca* requires that both enantiomers are present within the crystal.

The chirality originates about the bond between the platinum center and the phenanthridine nitrogen atom (Pt–N_P) and can be classified according to the conventions of axial chirality.[29,30] Viewed along the N_{ammine}–Pt–N_P vector, the platinum coordination plane lies in front of the perpendicular plane of the phenanthridine ring. Priority is assigned according to atomic number and degree of substitution. The direction in which the front ring needs to be rotated so as to have the priority substituent of the front plane coincide with the priority substituent of the back plane dictates the stereochemistry. Clockwise rotation is denoted *P* and counterclockwise rotation *M*. The different enantiomers of phenanthriplatin are shown in Figure 4.

The structure of **7** (Figure 3), the triflate salt of pyriplatin, also displays expected bond lengths and angles. In this complex, unlike **1**, the line connecting the platinum atom and the nitrogen atoms of the pyridine and the *trans* ammine is essentially contained by the plane of the *N*-heterocycle. The ring deviates significantly, however, from a perpendicular orientation with respect to the platinum coordination plane. The dihedral angle of 60° between the pyridine and the coordination plane is consistent with the angle of 56° observed for *trans*-[Pt(pyridine)$_2$Cl$_2$]. Details of the determination of the structure of a nonmerohedral trilling of this latter compound

dx.doi.org/10.1021/ja4125115 | J. Am. Chem. Soc. 2014, 136, 2126–2134

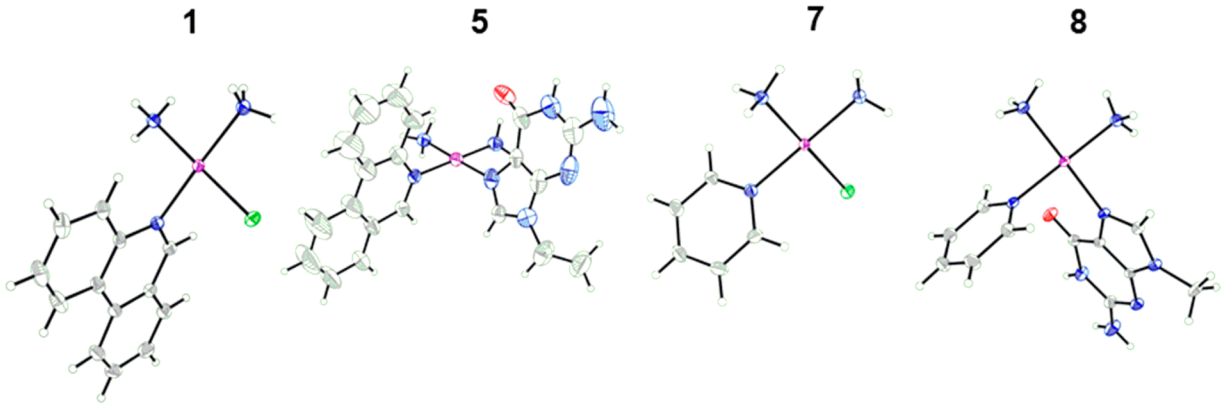

Figure 3. Molecular diagrams of the platinum complexes from the crystal structures of **1**, **5**, **7**, and **8** with thermal ellipsoids drawn at the 50% probability level. Color code: N blue, O red, C gray, Cl green, Pt magenta, H open circles.

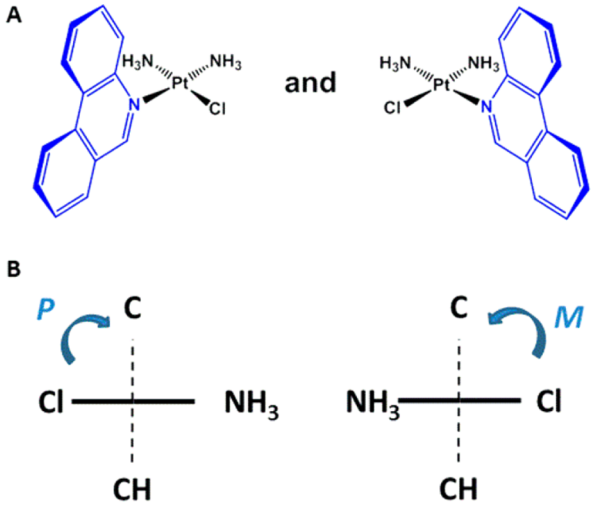

Figure 4. (A) The enantiomers of phenanthriplatin and (B) the convention used to classify them. In part B, the complex is viewed along the ammine−platinum−phenanthridine vector. The coordination plane is shown as a darkened line, and the phenanthridine plane as a dashed line.

are presented in the Supporting Information. Given the lack of steric or electronic factors to enforce strict perpendicularity between the pyridine ring and the coordination plane, the angle in both cases is most likely dictated by crystal packing interactions.

The solution and refinement of the structure of **8** (Figure 3) proceeded smoothly, except for the presence of a void about the 0, 0, 1/4 special position containing disordered electron density. The density could not be successfully modeled as either a molecule of DMF, diethyl ether, or a 1:1 disorder of the two, any of which would be consistent with the 41 e^- within the void. The SQUEEZE algorithm was applied to account for this disordered solvent. One DMF molecule disordered across each of the 4 voids of 228 $Å^3$ within the unit cell ($Z = 8$) would be consistent with the combustion analysis results obtained from this material. The pyridine and 9-methylgunanine rings are both canted in the same direction by 19° and 23°, respectively.

The structure of **5**, the product of the reaction of activated **1** with 9-ethylguanine, was also solved (Figure 3). The salt crystallized along with one water molecule, located on the 2-fold proper rotation axis, and one disordered acetone molecule. The presence of 0.5 equiv of water is consistent with the elemental analysis of this compound. The acetone present in the structure is not observed during combustion analysis and is probably removed during the vacuum drying of the substance. The phenanthridine ligands lie parallel to the *ac* plane, and the 9-ethylguanine ligands and the platinum coordination plane lie perpendicular to this crystallographic plane. The phenanthridine and 9-ethylguanine ligands of the square-planar complex cation are coordinated *cis* to each other. The former is oriented essentially perpendicular to the coordination plane but the latter is canted by 23°, such that the guanine carbonyl oxygen approaches the ammine coordinated *cis* to it. The O···N distance is 3.19 Å.

Nuclear Overhauser Effect NMR Experiments. Preirradiation at the frequency of the $H8_G$ signal in solutions of **6** and **8** induced perturbations in the signals of those protons that interact with $H8_G$ in a through-space manner. In the difference spectrum of **8**, obtained as described above, negative peaks were seen arising from the CH_3 protons of the 9-methyl group as well as the *ortho* hydrogen atoms of the pyridine ring (Figure S26). In the difference spectrum of **6**, a negative peak was again seen for the CH_3 protons of the 9-methyl group. Negative peaks were also observed for H6 and H7 of the phenanthridine ring (Figure S27) owing to their close proximity to $H8_G$. The ROESY spectrum of **6** also confirms the presence of the through-space interaction between $H8_G$ and H6 of the phenanthridine ring (Figure S28).

Molecular Modeling. *Molecular Mechanics.* Geometry optimizations were performed on two conformational isomers of **5** that are related by a 180° rotation about the Pt−N_P bond. In calculations in which the starting geometry had both *N*-heterocyclic ligands perpendicular to the coordination plane, optimization did not significantly alter the geometries of either of the conformers, which exhibited a negligible difference in strain energy. An overlay of the optimized structures of both conformers is shown in Figure 5.

Density Functional Theory. More rigorous geometry optimization using DFT methods reproduced the canting of the alkylguanine ligand that was observed in the crystal structure of **5** (Figure 6). In the gas phase, the distance of 2.72 Å between the carbonyl oxygen and the ammine nitrogen is sufficiently small to propose the presence of an intramolecular hydrogen bond. The calculations were also carried out with implicit aqueous solvation. As expected, the interaction between the carbonyl oxygen atom and the ammine nitrogen atom is attenuated, but the resulting O···N distance of 2.86 Å

dx.doi.org/10.1021/ja4125115 | *J. Am. Chem. Soc.* 2014, 136, 2126−2134

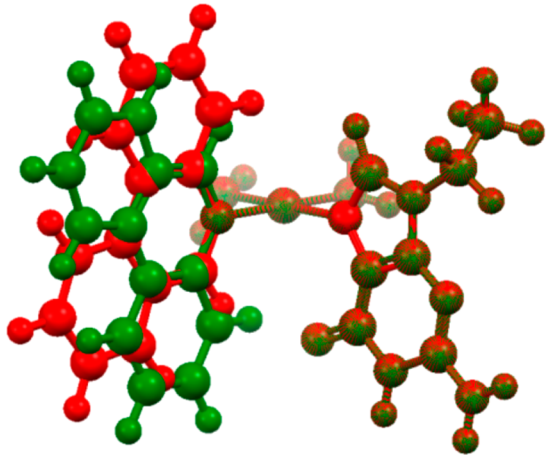

Figure 5. Overlay of the molecular mechanics optimized geometries obtained by setting the aromatic ligands perpendicular to the platinum coordination plane and rotating 180° about the platinum−phenanthridine bond.

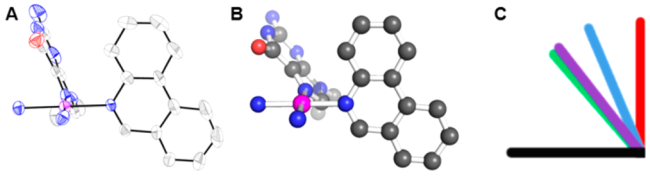

Figure 6. The canting of the guanine ring in (A) the crystal structure and (B) the DFT-optimized structure of **5**. Color code: N blue, O red, C gray, Pt magenta, H atoms omitted for clarity. (C) Schematic representation of the dihedral angle formed between the platinum coordination plane (black) and the phenanthridine ring of **5** in the MM calculations (red), the crystal structure (blue), the DFT calculations with implicit water solvation (purple), and the DFT calculations in the gas phase (green).

suggests that the interaction persists even in the presence of highly polar solvents.

DISCUSSION

The Chirality of Phenanthriplatin. Studies with pyriplatin showed that this compound has a spectrum of activity that differs significantly from those of the clinically employed platinum anticancer drugs.[10] The low potency of pyriplatin prompted a search for molecules that maintain this distinct spectrum of activity, but display higher activity. Phenanthriplatin was developed as the result of a systematic variation of the *N*-heterocyclic amine ligand, Am, of *cis*-$[Pt(NH_3)_2(Am)Cl]^+$.[6] It was found to be 7−40-fold more potent that cisplatin across a variety of cell lines, and the distinct spectrum of activity was maintained.

In an effort to better understand the mechanism of anticancer action of phenanthriplatin, we sought to investigate the structures of the adducts formed by phenanthriplatin and analogs of guanosine. For these studies, the triflate salt of the *cis*-$[Pt(NH_3)_2(Am)Cl]^+$ cation was prepared to facilitate subsequent synthetic steps. In the process of analyzing the solid state structure of the compound, however, we realized an aspect of the structure of this complex that had previously gone unnoticed: in the solid state, the complex cation is chiral. The centrosymmetric space group of the structure requires that both enantiomers be present in the crystal in equal portions. The chirality arises from the asymmetry of the phenanthridine ring about the coordination plane to which it is perpendicular. This asymmetry is not present in the pyridine derivative, pyriplatin.

The importance of chirality in pharmacological agents has long been recognized. Different enantiomers of pharmaceutics typically display different activity because these molecules interact with biological systems that are inherently chiral. One example of direct relevance to the field of platinum anticancer research is oxaliplatin, which contains only one enantiomer in the form that is marketed for clinical use.[31] The *R,R* isomer of *trans*-diaminocyclohexaneoxalatoplatinum(II) has greater activity than that of the enantiomeric *S,S* form.[32] If phenanthriplatin is indeed a racemic mixture of two stable enantiomers, then one might have significantly different activity than the other.

It is crucial to realize, however, that the two enantiomers can interconvert via rotation about $Pt-N_P$. If rotation about this bond is rapid at ambient or physiological temperatures, then the complex is effectively achiral. As will be discussed below, in addition to implications for the enantiomeric resolution of the compound, asymmetry of the phenanthridine ligand about the platinum coordination plane also has implications for its interaction with DNA. Investigation of the phenanthridine rotation is similar in nature to studies that have been carried out on models and retro-models of 1,2-d(GpG) intrastrand cross-links formed by bifunctional platinum compounds.[33] This similarity arises from the fact, as will become important below, that both the phenanthridine ligand and guanine derivatives coordinate in a manner that is asymmetric about the platinum coordination plane. The chirality present in models of the intrastrand $[Pt(NH_3)_2\{d(GpG)\}]$ adduct was first recognized by Cramer et al.[34] The phenomenon has subsequently been investigated in great detail by Marzilli, Natile, and co-workers, among others.[33]

Dynamic NMR spectroscopy is a method ideally suited to investigate whether rotation about a chemical bond is hindered.[35] Rotation about $Pt-N_P$ in phenanthriplatin interconverts two enantiomers with identical NMR properties, however, and so this dynamic process will induce no change in the line shape of the spectrum, regardless of the rate at which it occurs. Accordingly, the room temperature ^1H NMR spectrum of **1** shows a single set of well-defined resonances. The signals in the aromatic region are particularly sharp, and the breadth of the signals arising from the two ammines is due to a combination of quadrupolar relaxation from ^{14}N and coupling to CSA-broadened ^{195}Pt. To investigate rotation about the $Pt-N_P$ bond, the rotamers must be rendered diastereomeric. This goal was accomplished by replacing the two ammine ligands with the enantiomerically pure *R,R*-diaminocyclohexane (DACH) chelate. The C_2 symmetry of this ligand ensures that the coordination sites *trans* to the two coordinated nitrogen atoms are chemically equivalent. In the room temperature ^1H NMR spectrum of **2**, the signals arising from the protons on the aromatic ring are all cleanly doubled (Figures 1 and S19). Moreover, raising the temperature of the sample induces broadening, coalescence, and subsequent sharpening of the signals (Figure S19). This behavior is consistent with the presence of two rotamers that interconvert rapidly on the NMR time scale at elevated temperature. The conformations of these two rotamers are equivalent to those of the enantiomers of phenanthriplatin, i.e. *M* and *P*, giving rise to (*R,R*)*M* and (*R,R*)*P* diastereomers.

Detailed information about the energetics of the rotamer interconversion can be obtained by simulating the experimental

dx.doi.org/10.1021/ja4125115 | J. Am. Chem. Soc. 2014, 136, 2126−2134

line shapes obtained at different temperatures. The fit of the simulation to the experimental data can be optimized by varying k, the rate constant for interconversion. These k values obtained at different temperatures can be used to construct an Eyring plot from which the activation parameters for the interconversion can be extracted. The Gibbs free energy of activation for the interconversion of the $(R,R)M$ and $(R,R)P$ diastereomers of **2** at room temperature, $\Delta G_{298.15}^{\ddagger}$, was 70 kJ mol^{-1}, and the corresponding rate constant at this temperature was 3.2 s^{-1}. The inverse of this rate constant reveals that 63% of a diastereomerically pure sample of **2** would racemize within about 300 ms of dissolution at ambient conditions.

This result would appear to indicate that rotation about the Pt−N_P bond in phenanthriplatin is rapid. The validity of this conclusion, however, rests on the accuracy with which **2** models the structure of **1**. The most significant difference of relevance to the discussion at hand is in the N−Pt−N angle formed by either the ammines of **1** or the DACH of **2**. The former, obtained from the crystal structure of **1**, is 89.1°, and the latter, from the crystal structure of oxaliplatin, is 83.5°.[31,36] The smaller angle enforced by the chelator relieves the steric interactions that provide a barrier to rotation of the phenanthridine ring. The barrier obtained with **2**, therefore, provides an *upper* estimate to the rate of rotation in phenanthriplatin. It is possible that the rotation about Pt−N_P in phenanthriplatin will be sufficiently slower that enantiomeric resolution may be possible.

To obtain a diastereomeric analog of **1** in which the N−Pt−N angle formed by the ammines is left unperturbed, **4** was prepared. The addition of a second Pt−N_P bond as a center of chirality creates (P,M), (M,P), (P,P), and (M,M) conformational isomers. The (P,P) and (M,M) designations describe a meso compound, and the (P,M) and (M,P) rotamers are enantiomers. Hindered rotation about the Pt−N_P bonds would, therefore, give rise to two sets of signals. Using a dynamic NMR analysis analogous to that described above for **2**, activation parameters can be extracted (Table 1, Figure S25). In addition to adding a second chiral center, however, the second phenanthridine ligand may introduce steric bulk that inhibits Pt−N_P rotation to a degree greater than in **1**.

To assess the influence of the *cis* disposition of two phenanthridine rings on Pt−N_P rotation, **3** was prepared. The set of conformers listed for **3** is also present for **4**, but the presence of the *R,R*-DACH ligand renders all four rotamers diastereomeric: $(R,R)(P,M)$, $(R,R)(M,P)$, $(R,R)(P,P)$, and $(R,R)(M,M)$. Dynamic NMR spectroscopy again reveals the activation parameters for interconversion (Table 1) through a simulation of the line shapes of the four distinct sets of ^{1}H NMR signals that coalesce on heating (Figure S24).

A comparison of the results obtained from the dynamic NMR experiments on **2**−**4** is shown in Scheme 1. Upon transitioning from **2** to **3**, the addition of the extra phenanthridine ligand raised the barrier to rotation, but the lifetime only changed by a factor of 1.7. Exchanging the chelating DACH present in **3** for the two ammine ligands in **4** increased the lifetime by an order of magnitude. Even so, the lifetime of a given diastereomer of **4** is about 5 s. Importantly, unlike **2**, **4** provides an upper estimate of the barrier to rotation in phenanthriplatin. The results with **3** and **2** indicate that transitioning from **4** to **1** will lower the barrier to phenanthridine rotation. It is, therefore, reasonable to conclude that rotation about the Pt−N_P bond in phenanthriplatin is rapid on the pharmacological time scale and that enhanced activity

Scheme 1. Comparison of the Rates of Interconversion of Diastereomeric Isomers of 1−4

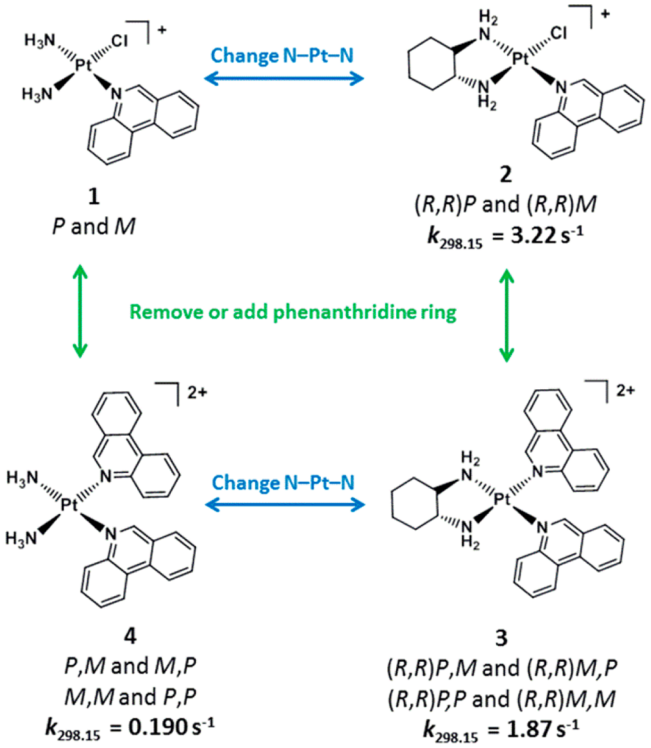

cannot be obtained by isolating and administering one of the isolated enantiomers. The rotation about this bond does, however, play a significant role in the interaction of **1** with DNA.

Interactions with 9-Alkylguanine. The interaction of phenanthriplatin with DNA can be modeled by preparing complexes with the formula *cis*-[Pt(NH_3)$_2$(phenanthridine)(9-alkylguanine)]$^{2+}$. Compounds **6** and **5** (Chart 2) were prepared using 9-methyl- and 9-ethylguanine, respectively. The guanine is expected to coordinate to the platinum through the N7 position. This mode of coordination is corroborated by the shift in the $H8_G$ ^{1}H NMR signal observed on binding to the platinum.[37] As a result of this coordination geometry, the guanine ring is asymmetric about the coordination plane. The bond between the platinum center and the N7 of the guanine (Pt−N_G) acts as a center of chirality in the same manner as Pt−N_P. Multiplicity in the ^{1}H signals was expected to arise due to the slow interconversion of (P_P,M_G), (M_P,P_G), (P_P,P_G), and (M_P,M_G), where the subscripts indicate the coordinate bond to either phenanthridine (P) or 9-alkylguanine (G). Surprisingly, however, only a single set of signals was observed (Figure S8). Cooling an NMR sample to −60 °C did not induce any decoalescence or broadening (Figure S22). In these molecules, therefore, either intramolecular rotation is occurring significantly more rapidly than in complexes **1**−**4** or one particular set of conformers is preferentially formed. Note that, for instance, (P_P,P_G) and (M_P,M_G) are enantiomers and would produce identical NMR spectra.

Through-space dipolar interactions between NMR active nuclei provide an ideal means with which to probe three-dimensional molecular structure in solution. Before investigating the more complex phenanthridine-containing compounds, however, a simpler pyriplatin analog was prepared and studied. In **8**, the pyridine ring is symmetric about the platinum

dx.doi.org/10.1021/ja4125115 | J. Am. Chem. Soc. 2014, 136, 2126−2134

coordination plane and so the platinum−pyridine bond is not a center of chirality. The chirality about Pt−N_G produces enantiomers but not diastereomers. In the crystal structure of **8**, there are 2 sets of protons that are close enough to suggest that a nuclear Overhauser effect (NOE) will occur involving $H8_G$: the CH_3 of the 9-methyl group (2.52 Å) and the *ortho* protons from the pyridine ring (3.56 Å). The methyl group provides a particularly convenient internal standard because the rigidity of the guanine ring ensures that the methyl protons will stay in close proximity to $H8_G$ regardless of the relative orientation of the pyridine and guanine rings. A ^{1}H saturation transfer NMR experiment was carried out with preirradiation at the frequency of the $H8_G$ signal and revealed a through-space interaction between $H8_G$ and the 9-methyl protons as well as the *ortho* protons of the pyridine ring (Figure S26).

In the (M_P,P_G) isomer of **6**, as well as the enantiomeric (P_P,M_G), $H8_G$ and $H6_P$ are on the same side of the coordination plane. In (P_P,P_G) and (M_P,M_G), which are diastereomers of the first pair, $H8_G$ and $H4_P$ are on the same side of the platinum coordination plane. Only those protons that are on the same side of the platinum coordination plane as $H8_G$ are expected to undergo through-space interactions with this nucleus. When a saturation transfer experiment analogous to that described for **8** was conducted with **6**, an interaction was observed between $H8_G$ and the 9-methyl protons, as expected, and with the $H6_P$ proton. No significant interaction was observed with $H4_P$ (Figure S27). Moreover, an interaction was also seen with $H7_P$, further confirming that the (M_P,P_G)/(P_P,M_G) enantiomeric pair is preferentially formed in solution over the (P_P,P_G)/(M_P,M_G) pair. A though-space interaction was also observed in the ROESY spectrum (Figure S28). A crystal structure of **5** was solved (Figure 3), and it also showed only the presence of (M_P,P_G) and (P_P,M_G). The centrosymmetry of the space group $C2/c$ in which the complex crystallized requires the presence of both enantiomers.

Molecular mechanics calculations were initially performed to interrogate the origin of the diastereoselectivity exhibited by **5** and **6**. Calculations in which the aromatic ligands were set perpendicular to the coordination plane (Figure 5) revealed little energetic difference between the two diastereomeric forms. Inspection of the crystal structure of **5**, however, reveals that the guanine ligand is not perpendicular to the coordination plane. Rather, it cants so as to direct the carbonyl oxygen toward the *cis*-coordinated ammine. The O···N distance of 3.19 Å is too long to constitute a formal intramolecular hydrogen bond in the solid state, but such an interaction may occur in solution. A similar interaction between the carbonyl of a pyriplatin-platinated guanosine and the *cis* ammine of the platinum complex was observed in the crystal structure of pyriplatin-platinated dodecamer duplex DNA.[7]

DFT geometry optimization was able to reproduce the canting of the 9-alkylguanine. In the optimized gas phase geometry, the O···N distance is 2.72 Å. Inclusion of implicit aqueous solvation weakens the interaction somewhat, but the O···N separation remains short at 2.86 Å. The origin of the diastereoselectivity appears to result from this canting of the guanine ligand, which relieves steric congestion over one face of the platinum complex. One side of the phenanthridine ligand has a greater degree of steric bulk in the vicinity of the platinum center than the other, as illustrated in Figure 6. In the favored diastereomer, this bulkier portion of the phenanthridine is directed toward the vacant space formed by the canting of the guanine. It remains to be seen whether the conformational preference is maintained in full length DNA polymers or during complexation with proteins that recognize platinum lesions.

As a final comment, we note that if rotation about the Pt−N bonds in phenanthriplatin were not rapid, then different diastereomeric forms of the platinum adduct could be kinetically trapped regardless of the energetic preference that might exist for one conformer. Instead, the unhindered bond rotation established above allows the complex to assume the thermodynamically favorable conformation, regardless of the manner in which it initially binds to the 9-alkylguanine.

■ CONCLUSIONS

The solid state structure of phenanthriplatin highlights the fact that asymmetry of the phenanthridine ligand about the platinum coordination plane results in chirality. The two enantiomers are, however, interconvertible via rotation about the Pt−N_P bond. The use of model compounds with diastereomeric rotamers provides evidence that rotation about this bond in phenanthriplatin is rapid, eliminating any need to isolate and administer an enantiomerically pure compound. Rapid rotation about the this bond also prevents the kinetic resolution of diastereomers in complexes of the type *cis*-$[Pt(NH_3)_2$(phenanthridine)(9-alkylguanine)$]^{2+}$, which mimic the interaction of phenanthriplatin with DNA. Rather, it permits the more stable diastereomer to form. The (M_P,P_G) and (P_P,M_G) diastereomers observed in both solution and the solid state are those in which the $H8_G$ and $H6_P$ are located on the same side of the platinum coordination plane. The experimental data described above indicate that interaction between the guanine carbonyl and *cis*-coordinated ammine determines the preferential diastereomer formation.

■ ASSOCIATED CONTENT

Supporting Information

Experimental section, NMR spectra, VT NMR spectra, simulated line shapes and associated Eyring plots, crystallographic details for *trans*-$[Pt(pyridine)_2Cl_2]$, refinement details for **1**, **5**, **7**, and **8**, CIFs for **1**, **5**, **7**, and **8**. This information is available free of charge via the Internet at http://pubs.acs.org.

■ AUTHOR INFORMATION

Corresponding Author

lippard@mit.edu

Notes

The authors declare the following competing financial interest(s): S.J.L. has a financial interest in Blend Therapeutics, which aims to take platinum compounds to the clinic.

■ ACKNOWLEDGMENTS

This work is supported by the NCI under Grant CA034992. Y.-R. Zheng is thanked for his assistance in preparing line diagrams of enantiomeric and diastereomeric species. I. A. Riddell is thanked for many helpful discussions and suggestions.

■ REFERENCES

(1) O'Dwyer, P. J.; Stevenson, J. P.; Johnson, S. W. In *Cisplatin - Chemistry and Biochemistry of a Leading Anticancer Drug*; Lippert, B., Ed.; Verlag Helvetica Chimica Acta: Zürich, Switzerland, 1999; p 31.
(2) Wheate, N. J.; Walker, S.; Craig, G. E.; Oun, R. *Dalton Trans.* **2010**, *39*, 8113.
(3) Kelland, L. *Nat. Rev. Cancer* **2007**, *7*, 573.
(4) Lovejoy, K. S.; Lippard, S. J. *Dalton Trans.* **2009**, 10651.

(5) Johnstone, T. C.; Wilson, J. J.; Lippard, S. J. *Inorg. Chem.* **2013**, *52*, 12234.
(6) Park, G. Y.; Wilson, J. J.; Song, Y.; Lippard, S. J. *Proc. Natl. Acad. Sci. U.S.A.* **2012**, *109*, 11987.
(7) Lovejoy, K. S.; Todd, R. C.; Zhang, S.; McCormick, M. S.; D'Aquino, J. A.; Reardon, J. T.; Sancar, A.; Giacomini, K. M.; Lippard, S. J. *Proc. Natl. Acad. Sci. U.S.A.* **2008**, *105*, 8902.
(8) Todd, R. C.; Lippard, S. J. *J. Inorg. Biochem.* **2010**, *104*, 902.
(9) Wang, D.; Zhu, G.; Huang, X.; Lippard, S. J. *Proc. Natl. Acad. Sci. U.S.A.* **2010**, *107*, 9584.
(10) Lovejoy, K. S.; Serova, M.; Bieche, I.; Emami, S.; D'Incalci, M.; Broggini, M.; Erba, E.; Gespach, C.; Cvitkovic, E.; Faivre, S.; Raymond, E.; Lippard, S. J. *Mol. Cancer Ther.* **2011**, *10*, 1709.
(11) Cleare, M. J.; Hoeschele, J. D. *Bioinorg. Chem.* **1973**, *2*, 187.
(12) Johnstone, T. C.; Park, G. Y.; Lippard, S. J. *Anticancer Res.* **2014**, *34*, 471.
(13) Dhar, S.; Lippard, S. J. In *Bioinorganic Medicinal Chemistry*; Alessio, E., Ed.; Wiley-VCH Verlag GmbH & Co. KGaA: Weinheim, Germany, 2011; p 79.
(14) Johnstone, T. C.; Alexander, S. M.; Lin, W.; Lippard, S. J. *J. Am. Chem. Soc.* **2014**, *136*, 116.
(15) Sherman, S. E.; Lippard, S. J. *Chem. Rev.* **1987**, *87*, 1153.
(16) Pople, J. A. *High-resolution nuclear magnetic resonance*; McGraw-Hill: New York, 1959.
(17) Kurland, R. J.; Rubin, M. B.; Wise, W. B. *J. Chem. Phys.* **1964**, *40*, 2426.
(18) Kost, D.; Carlson, E. H.; Raban, M. *J. Chem. Soc. D* **1971**, 656.
(19) Bain, A. D.; Rex, D. M.; Smith, R. N. *Magn. Reson. Chem.* **2001**, *39*, 122.
(20) Bain, A. D. *MEXICO*, **2002**, Hamilton, ON.
(21) Frisch, M. J.; Trucks, G. W.; Schlegel, H. B.; Scuseria, G. E.; Robb, M. A.; Cheeseman, J. R.; Montgomery, J. A., Jr.; Vreven, T.; Kudin, K. N.; Burant, J. C.; Millam, J. M.; Iyengar, S. S.; Tomasi, J.; Barone, V.; Mennucci, B.; Cossi, M.; Scalmani, G.; Rega, N.; Petersson, G. A.; Nakatsuji, H.; Hada, M.; Ehara, M.; Toyota, K.; Fukuda, R.; Hasegawa, J.; Ishida, M.; Nakajima, T.; Honda, Y.; Kitao, O.; Nakai, H.; Klene, M.; Li, X.; Knox, J. E.; Hratchian, H. P.; Cross, J. B.; Adamo, C.; Jaramillo, J.; Gomperts, R.; Stratmann, R. E.; Yazyev, O.; Austin, A. J.; Cammi, R.; Pomelli, C.; Ochterski, J. W.; Ayala, P. Y.; Morokuma, K.; Voth, G. A.; Salvador, P.; Dannenberg, J. J.; Zakrzewski, V. G.; Dapprich, S.; Daniels, A. D.; Strain, M. C.; Farkas, O.; Malick, D. K.; Rabuck, A. D.; Raghavachari, K.; Foresman, J. B.; Ortiz, J. V.; Cui, Q.; Baboul, A. G.; Clifford, S.; Cioslowski, J.; Stefanov, B. B.; Liu, G.; Liashenko, A.; Piskorz, P.; Komaromi, I.; Martin, R. L.; Fox, D. J.; Keith, T.; Al-Laham, M. A.; Peng, C. Y.; Nanayakkara, A.; Challacombe, M.; Gill, P. M. W.; Johnson, B.; Chen, W.; Wong, M. W.; Gonzalez, C.; Pople, J. A. *Gaussian 03*; Gaussian, Inc.: Pittsburgh, PA, 2003.
(22) Rappé, A. K.; Casewit, C. J.; Colwell, K. S.; Goddard, W. A., III; Skiff, W. M. *J. Am. Chem. Soc.* **1992**, *114*, 10024.
(23) Johnstone, T. C.; Lippard, S. J. *Polyhedron* **2013**, *52*, 565.
(24) Neese, F. *Wiley Interdiscip. Rev.: Comput. Mol. Sci.* **2012**, *2*, 73.
(25) Becke, A. D. *Phys. Rev. A* **1988**, *38*, 3098.
(26) Perdew, J. P. *Phys. Rev. B* **1986**, *33*, 8822.
(27) Pantazis, D. A.; Chen, X.-Y.; Landis, C. R.; Neese, F. *J. Chem. Theory Comput.* **2008**, *4*, 908.
(28) Giandomenico, C. M.; Abrams, M. J.; Murrer, B. A.; Vollano, J. F.; Rheinheimer, M. I.; Wyer, S. B.; Bossard, G. E.; Higgins, J. D., III. *Inorg. Chem.* **1995**, *34*, 1015.
(29) Moss, G. P. *Pure Appl. Chem.* **1996**, *68*, 2193.
(30) Biagini, M. C.; Ferrari, M.; Lanfranchi, M.; Marchiò, L.; Pellinghelli, M. A. *J. Chem. Soc., Dalton Trans.* **1999**, 1575.
(31) Johnstone, T. C. *Polyhedron* **2014**, *67*, 429.
(32) Dabrowiak, J. C. *Metals in Medicine*; Wiley: Hoboken, 2009; p 109.
(33) Natile, G.; Marzilli, L. G. *Coord. Chem. Rev.* **2006**, *250*, 1315.
(34) Cramer, R. E.; Dahlstrom, P. L. *J. Am. Chem. Soc.* **1979**, *101*, 3679.
(35) Jackman, L. M.; Cotton, F. A.; Adams, R. D. *Dynamic nuclear magnetic resonance spectroscopy*; Academic Press: New York, 1975.
(36) Bruck, M. A.; Bau, R.; Noji, M.; Inagaki, K.; Kidani, Y. *Inorg. Chim. Acta* **1984**, *92*, 279.
(37) Lemaire, D.; Fouchet, M.-H.; Kozelka, J. *J. Inorg. Biochem.* **1994**, *53*, 261.